Quantitative Comparison of Zero-Loss and Conventional Electron Diffraction from Two-Dimensional and Thin Three-Dimensional Protein Crystals

Koji Yonekura,* Saori Maki-Yonekura,* and Keiichi Namba*†

*Protonic NanoMachine Project, ERATO, JST, 3-4 Hikaridai, Seika 619-0237 Japan; and †Advanced Technology Research Laboratories, Matsushita Electric Industrial Company, Ltd., 3-4 Hikaridai, Seika 619-0237 Japan

ABSTRACT The scattering cross-section of atoms in biological macromolecules for both elastically and inelastically scattered electrons is ~100,000 times larger than that for x-ray. Therefore, much smaller (<1 μm) and thinner (<0.01 μm) protein crystals than those used for x-ray crystallography can be used to analyze the molecular structures by electron crystallography. But, inelastic scattering is a serious problem. We examined electron diffraction data from thin three-dimensional (3-D) crystals (600–750 Å thick) and two-dimensional (2-D) crystals (~60 Å thick), both at 93 K, with an energy filtering electron microscope operated at an accelerating voltage of 200 kV. Removal of inelastically scattered electrons significantly improved intensity data statistics and $R_{Friedel}$ factor in every resolution range up to 3-Å resolution. The effect of energy filtering was more prominent for thicker crystals but was significant even for thin crystals. These filtered data sets showed better intensity statistics even in comparison with data sets collected at 4 K and an accelerating voltage of 300 kV without energy filtering. Thus, the energy filter will be an effective and important tool in the structure analysis of thin 3-D and 2-D crystals, particularly when data are collected at high tilt angle.

INTRODUCTION

Electron crystallography has been widely applied to determine the structures of biological macromolecules. When well ordered 2-D crystals are available, the attainable resolution can be as high as 3 Å or even higher, where peptide chain tracing is possible (Henderson et al., 1990; Kühlbrandt et al., 1994; Kimura et al., 1997; Nogales et al., 1998; Murata et al., 2000). This method is particularly powerful for membrane proteins because they are naturally localized in the 2-D space of the membrane monolayer. For high-resolution structure analysis, although both amplitudes and phases can be obtained from the Fourier transform of image data, it is far better to use amplitudes from electron diffraction patterns because of their superior accuracy and no need of correction for the contrast transfer function of the electron microscope. Relatively low electron dose required for recording an electron diffraction pattern, which can be less than one-tenth of the dose required for taking an image, gives a further advantage in reducing radiation damage.

Structure analysis essentially uses only elastically scattered electrons for a weak-phase object such as proteins, which consist of only light atoms. Inelastically scattered electrons, which lost some energy through interactions with a specimen, contribute to high background noises in electron diffraction patterns, especially at low resolution. Inelastic scattering from ice or sugar in which samples are embedded is also a major source of such background noise. There are more than three times more inelastic electrons than elastic ones in electrons scattered by ice (Angert et al., 1996). Energy filtering can remove such inelastically scattered electrons effectively.

There have been studies on the effect of energy filtering in cryo-imaging of proteins (e.g., Langmore and Smith, 1992; Zhu et al., 1997; Angert et al., 2000), but few studies have dealt with quantitative characterization of its effect on electron diffraction data from protein crystals. An advantage in using electron diffraction from crystals over imaging for evaluating the effect of energy filtering is that quantitative analyses can be carried out for high-resolution data more easily and reliably. Toyoshima et al. (1998) briefly described an improved data quality of electron diffraction patterns obtained by using a γ-type energy filter (Taya et al., 1996) operated at an accelerating voltage 125 kV. Here, we report quantitative analyses of electron diffraction data obtained with and without energy filtering by using a HITACHI EF-2000 electron microscope, which is equipped with a γ-type energy filter and operated at an accelerating voltage of 200 kV. We used thin 3-D crystals (600–750 Å thick) and 2-D crystals (~60 Å thick) to see the effect of energy filtering on specimens with different thickness. We also compared these data with unfiltered data sets collected at an accelerating voltage of 300 kV to look into the advantage of higher voltage. The results clearly demonstrated that removal of inelastically scattered electrons significantly improved intensity data statistics and $R_{Friedel}$ factor in every resolution range at least up to 3-Å resolution.

Submitted August 20, 2001, and accepted for publication January 29, 2002.

Address reprint requests to Keiichi Namba, Protonic NanoMachine Project, ERATO, JST, 3-4 Hikaridai, Seika 619-0237 Japan. Tel.: 81-774-98-2543; Fax: 81-774-98-2575; E-mail: keiichi@crl.mei.co.jp.

0006-3495/02/05/2784/14 $2.00

MATERIALS AND METHODS

Sample preparation and electron microscopy

A core fragment of flagellin, F41 (molecular weight 41,300), from *Salmonella typhimurium* was prepared as described by Samatey et al. (2000) and was kindly given to us by F. A. Samatey. Thin 3-D crystals of F41 were

prepared as described by Samatey et al. (2000) with slight modifications. Briefly, a protein solution in 20 mM Tris-HCl, pH 7.8, was mixed with the same volume of a reservoir solution, 15% polyethylene glycol 6000, 2% 2-methyl-2,4-pentanediol, 0.1% trehalose, 0 to 5 mM NaCl, 20 mM Tris-HCl, pH 7.8. The final protein concentration is ~3 mg/mL. Crystallization was carried out by the hanging drop vapor diffusion method at 16°C. Thin 3-D crystals with sizes of 2 to 40 μm and thickness less than 0.1 μm (space group $P2_1$, $a = 51.8$ Å, $b = 36.5$ Å, $c = 118.7$ Å, $\beta = 90.8°$) were obtained after 1 to 2 weeks. To achieve a good transfer rate of the crystals on electron microscope grids, carbon-coated gold grids were placed on crystallization drops just after setting up crystallization (Auer et al., 1999) or a few hours before freezing (Vénien-Bryan et al., 2000). After an excess volume of solution was blotted off the grid with a filter paper, the grid was frozen rapidly by plunging it into liquid ethane.

2-D crystals of bacteriorhodopsin (bR) were prepared as described by Mitsuoka et al. (1999). The specimen was kindly given to us by Y. Fujiyoshi. The crystals on a carbon-coated grid were frozen in a partially hydrated state as described by Hirai et al. (1999).

These sample grids were mounted on an Oxford CT3500 cryoholder and examined with a HITACHI EF-2000 electron microscope, which is equipped with a γ-type energy filter (Taya et al., 1996) and a cold field emission gun operated at an accelerating voltage of 200 kV. This in-column energy filter has an electromagnet that makes electrons through and scattered from the specimen travel through the γ-shaped trajectories. An energy slit below the electromagnet was adjusted to select only electrons with energy loss less than 10 eV. With this setting of the slit, we can exclude most of electrons with plasmon loss in ice (Langmore and Smith, 1992) and carbon. Putting the slit in or out of the electron trajectories is achieved easily by a single action of a lever. At least two electron diffraction patterns were taken from the same crystal with and without energy filtering, respectively, using a low dose program we have developed for electron diffraction. As a control data set, we also collected electron diffraction data from these samples by using a JEOL JEM-3000SFF electron microscope, which is equipped with a liquid helium-cooled stage and a thermal field emission gun operated at an accelerating voltage of 300 or 200 kV. The specimen temperatures were 93 K in EF-2000 and 4 K in JEM-3000SFF, respectively. Electron diffraction patterns were recorded with a GATAN 2k × 2k slow scan charge-coupled device (SSCCD) camera. The total dose for recording an electron diffraction pattern was set to ~1 $e^-/Å^2$. A selected area aperture with a diameter of ~1.2 μm at the specimen plane was always used for data collection. The thickness of the F41 crystal was estimated from the optical density of the image of the crystal by using the relation between the specimen thickness and the ratio of the electron intensity transmitted through the specimen to that through the surrounding area (Misell and Brown, 1987). Assuming that the thickness of 2-D bR crystals is ~60 Å, that of the F41 crystals was estimated to be 600 to 750 Å, which corresponds to five to six layers of F41 molecules because the layer interval, which is the *c*-axis repeat of the crystal, is 118.7 Å (Samatey et al., 2001).

Analysis of diffraction patterns

Electron diffraction patterns were analyzed by using a slightly modified version of the Medical Research Council image processing programs (Mitsuoka et al., 1999; Baldwin and Henderson, 1984). The circular-symmetric and radially smoothed background and local undulations were subtracted from each diffraction pattern as described by Baldwin and Henderson (1984) and Mitsuoka et al. (1999). Integration of the diffraction intensity within each spot was carried out in two steps by a newly developed program. First, 2-D intensity profiles of spots within a given measurement box were averaged for strong spots to obtain an averaged peak profile for each diffraction pattern. Then, pixels with the intensity higher than 20% of the peak intensity in the averaged profile were regarded as the peak region and those with the intensity less than 5% as the background region. The pixels with the intensity between 5% and 20% of the peak intensity were regarded as boundaries and not used for integration. The integrated intensity, I, was calculated as,

$$I = \sum_{i=1}^{m} \rho_i - \frac{m}{n} \sum_{j=1}^{n} \rho_j, \quad (1)$$

in which ρ_i and ρ_j are the intensity (the CCD count) at the ith and jth pixel, respectively, and m and n are the number of pixels within the peak and background regions, respectively. Pixels with the intensity higher than 3σ of the average in the background region were excluded from averaging. Variance (σ^2) of each spot was calculated as,

$$\sigma^2 = A \times \sum_{i=1}^{m} \rho_i + m^2 \times A^2 \times \sigma_{BG}^2, \quad (2)$$

in which the first term is based on Poisson statistics, σ_{BG} is the standard deviation in the background region, and A represents the electron detection efficiency of the SSCCD camera. The electron detection efficiency was calibrated as 0.05 e^-/count for the SSCCD installed in JEM-3000SFF (pixel size of 24 μm) and 0.14 e^-/count for the one installed in EF-2000 (pixel size of 30 μm). For quantitative analysis of electron diffraction patterns, I/σ was calculated for all reflections by Eqs. 1 and 2, and scaled to electron count as,

$$A \times I/\sigma. \quad (3)$$

The values of I/σ in the following text and legends all represent those scaled to electron counts calculated by Eq. 3.

RESULTS

Effect of energy filtering on thin 3-D crystal

Typical examples of unprocessed electron diffraction patterns from a thin F41 crystal with (right, the first exposure) and without (left, the second exposure) energy filtering are shown in Fig. 1. Inelastically scattered electrons produced the background of a high intensity level especially at low resolution as seen normally in the unfiltered electron diffraction pattern (left). By filtering out such electrons, the background intensity level was remarkably reduced (right). The radial background profile (lower panel) clearly shows that the reduction in the background level is significant not only in low resolution as generally expected but also in high resolution beyond 3 Å.

2-D intensity profiles of three arbitrary selected spots marked in Fig. 1 are shown in Fig. 2. The background around the peak was high and noisy without energy filtering (left) but was significantly reduced and became smoother by energy filtering (right). Even for the spot at 3.5-Å resolution, the background level was reduced to a forth and the noise level was also reduced accordingly by energy filtering. The ratio of the integrated intensity of each Bragg spot to the background intensity integrated within the same area increased from 0.5 to 36.9 for the spot at 12.2-Å resolution, from 2.3 to 16.5 for that at 5.1-Å resolution, and from 0.9 to 2.7 for that at 3.5-Å resolution. Also, the peak width was larger without energy filtering (Fig. 2, *b* and *c*). These differences were not caused by radiation damage, because the peak profiles obtained from filtered electron diffraction patterns taken in the third exposure were shaper than those of unfiltered data in the second expo-

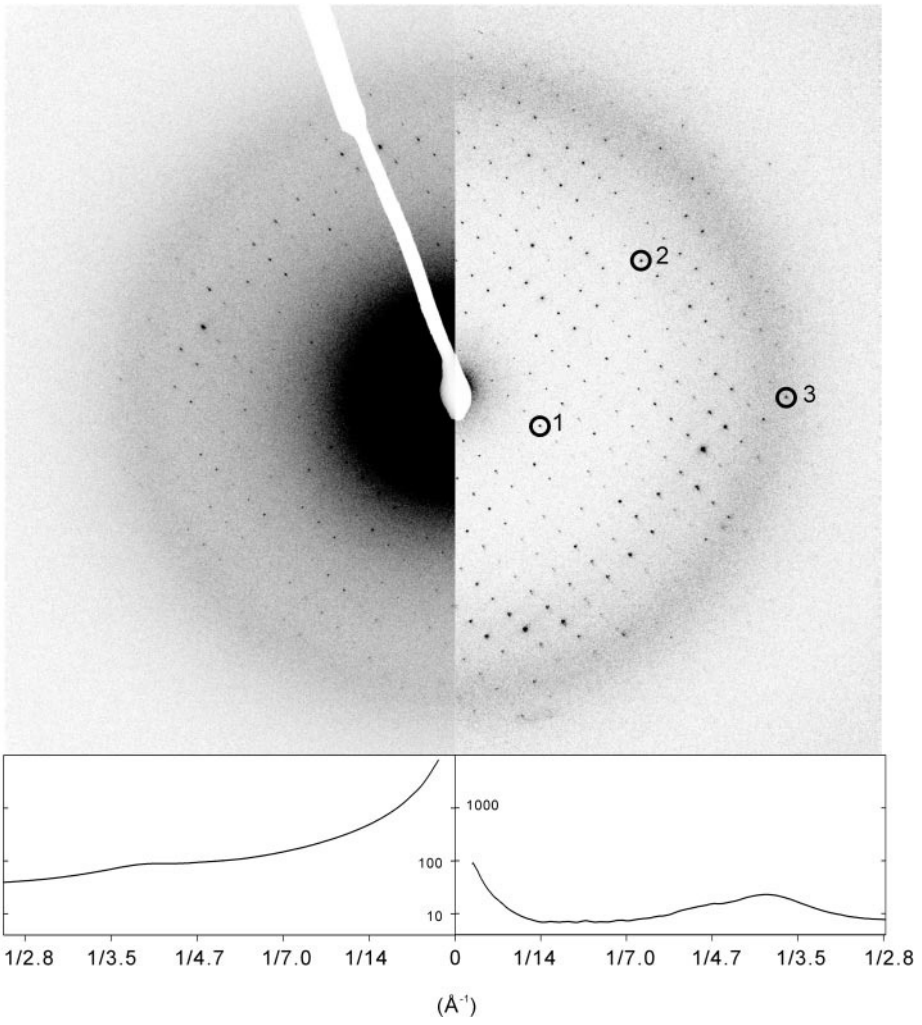

FIGURE 1 Side by side comparison of electron diffraction patterns from a thin 3-D crystal with and without energy filtering. The specimen is a thin 3-D crystal of F41 ($P2_1$, a = 51.8 Å, b = 36.5 Å, c = 118.7 Å, and β = 90.8°). The upper panels show diffraction images and the lower panels show radial background distributions (in log scale, CCD count). The left and right panels show diffraction data collected without and with energy filtering, respectively. The background intensity near the beam stop is almost 100 times higher on the left than that on the right. Even ~3-Å resolution, the background intensity without energy filtering is 5.5 times higher. Circles and numbers indicate representative reflections referred in Fig. 2. The broad circular intensity at ~1/3.65 $Å^{-1}$, which was identified to come from amorphous ice because it disappeared when the sample was warmed up to ~170 K, is more clearly seen with energy filtering.

sure (data not shown). By energy filtering, values of I/σ were also improved by ~2.8 times for the spot at 12.2-Å resolution by ~1.4 times for that at 5.1-Å resolution and by ~1.3 times for that at 3.5-Å resolution.

Fig. 3 shows the difference made by energy filtering in the distribution of I/σ as obtained from the same data as in Fig. 1. The results indicate that energy filtering can substantially improve I/σ in every resolution range. Even in the third exposure (Fig. 3 *c*), the I/σ values are much higher with energy filtering than those obtained without energy filtering in the second exposure (Fig. 3 *b*).

There was a slight decay in the intensity data obtained by the second and the third exposure by radiation damage, which can be seen by comparing the two data in Fig. 3, *a* and *c*, the first and the third shot, respectively. Therefore, it would be desirable to use only data sets taken in the first exposure with or without energy filtering. But, because the quality of crystal and its diffraction varies from crystal to crystal, the quantitative measure of the effect of energy filtering would be difficult to obtain from the first exposure data alone. Hence, we collected a pair of electron diffraction patterns with and without energy filtering from each crystal in either of the two different orders. In total, 10 pairs of electron diffraction patterns were collected and analyzed, five of which were taken with energy filtering first and without energy filtering second, and the remaining five were taken without energy filtering first and with energy filtering second. The intensity statistics obtained from 10 F41 crystals with and without energy filtering in this way are compared in Table 1 and Fig. 4. Table 1 shows the number of reflections within a given I/σ range, and the percentage fraction of reflections with I/σ higher than the lower limit of each I/σ range, both within each resolution range. Fig. 4 is a graphical display of the numbers in Table 1 for easier view of the difference between the two statistics obtained with and without energy filtering. The table and the figure both show clearly that values of I/σ from the filtered ones are much higher in all resolution ranges out to 3.0 Å.

The effect of energy filtering is most prominent in low-resolution range as expected. With energy filtering, 32.8% of total reflections have $I/\sigma > 7$ within a resolution of 15 Å, whereas no reflections have $I/\sigma > 7$ without energy filtering

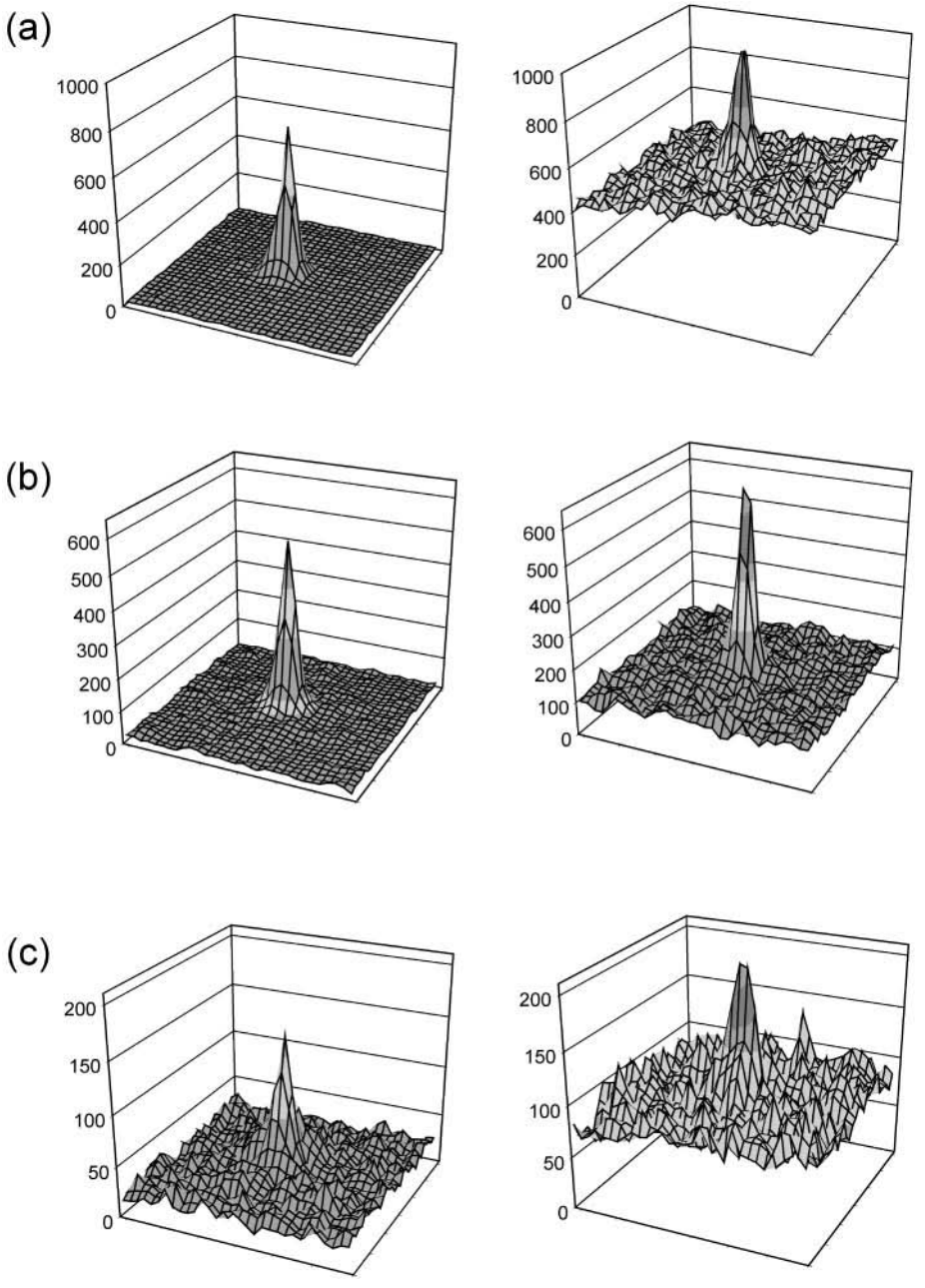

FIGURE 2 Comparison of peak and background intensity profiles with and without energy filtering. Intensity distributions are displayed in 3-D representation for the three reflections marked by circles in Fig. 1. (*a*) Spot 1 at 12.2-Å resolution; (*b*) spot 2 at 5.1-Å resolution; (*c*) spot 3 at 3.5-Å resolution. (*Left*) With energy filtering; (*Right*) without energy filtering. Total CCD counts of integrated Bragg spot intensity/integrated background intensity with and without energy filtering are: 4168/113 and 3388/6523 at 12.2 Å (spot 1); 3410/207 and 3341/1480 at 5.1 Å (spot 2); 1040/383 and 1099/1174 at 3.5 Å (spot 3). The values of I/σ with and without energy filtering are: 22.9 and 8.2 at 12.2 Å (spot 1); 19.3 and 13.7 at 5.1 Å (spot 2); 7.9 and 6.3 at 3.5 Å (spot 3). Without energy filtering, background intensities are higher and therefore their statistical noises are also higher, and it is true even at 3.5-Å resolution. The intensity unit corresponds to CCD count.

(Table 1), demonstrating a dramatic improvement in the intensity statistics by energy filtering. But, even in higher resolution, substantial improvements are observed by energy filtering. If we take only reflections with $I/\sigma > 5$ and compare the percentage fractions of reflections obtained with and without energy filtering in each resolution range, they are all increased by energy filtering: from 1.0% to 49.5% within 15 Å; from 26.2% to 81.2% in 15 to 7.5 Å; from 19.8% to 70.0% in 7.5 to 5.0 Å; from 24.3% to 49.8% in 5.0 to 3.7 Å; from 0.9% to 4.2% in 3.7 to 3.0 Å. If we collect reflections with $I/\sigma > 3$ within a resolution range of 3.7 to 3.0 Å, the percentage fraction is increased from 4.2% to 15.0%. These results clearly indicate that energy filtering is highly effective in improving the diffraction data statistics over all resolution ranges out to at least 3 Å. It would probably be so beyond 3-Å resolution as suggested by the comparison of the radial background curves shown in Fig. 1 obtained with and without energy filtering, in which the reduction of the background level by energy filtering amounts to ~80% even at 2.8 Å resolution, and a similar level of reduction appears to extend further beyond the resolution we analyzed in the present study.

Differences in the diffraction intensity between Friedel pairs were examined using the same 10 data sets obtained from F41 crystals. Table 2 shows the $R_{Friedel}$ factor of these data sets. Here, scaling of each data set was carried out by

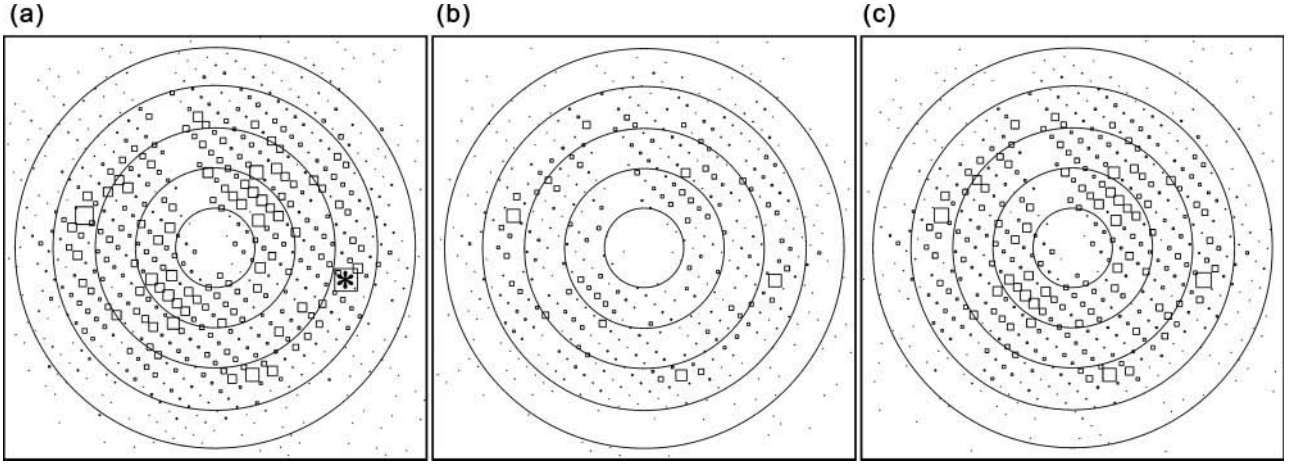

FIGURE 3 2-D plot of I/σ distributions comparing the quality of diffraction data with and without energy filtering. (*a*) From a diffraction pattern with energy filtering in the first exposure. (*b*) From a diffraction pattern without energy filtering in the second exposure. (*c*) From a diffraction pattern with energy filtering in the third exposure. All three data were collected from the same crystal of F41, and data shown in *a* and *b* are for the same diffraction data as those shown in Fig. 1. Each square represents each reflection with its size proportional to I/σ. Note that the size of each square (I/σ) in *a* and *c* are significantly larger than that of corresponding square in *b*. The size of each square in *c* is slightly smaller than that of corresponding square in *a* due to radiation damage in *c* by the previous two exposures for *a* and *b*. The square marked with an asterisk in *a* corresponds to the maximal I/σ of 50.6, which can be used as a scale. All reflections with $I/\sigma > 1$ are shown. Circles represent 15, 7.5, 5.0, 3.7, and 3.0 Å resolution, respectively.

using the sum of intensities of all the Friedel pairs. Energy filtering reduced the $R_{Friedel}$ factor by ~10 point within 15-Å resolution, by a few point beyond 15 Å, and by ~2 point even in 3.7- to 3.0-Å range. Because the standard $R_{Friedel}$ factor is strongly influenced by high intensity reflection data, the average of the $R_{Friedel}$ factors for individual Friedel pairs ($\Sigma\ R_{Friedel}$) was also calculated in each resolution range. Comparison of $R_{Friedel}$ and $\Sigma\ R_{Friedel}$ clearly revealed that the intensity differences between weak Friedel pairs became smaller by energy filtering.

TABLE 1 Data statistics of electron diffraction intensities from F41 crystals with or without energy filtering

	Resolution range (Å)					
	∞ ~ 15	15 ~ 7.5	7.5 ~ 5.0	5.0 ~ 3.7	3.7 ~ 3.0	Overall
$I/\sigma > 30$	0/0	12/1	1/0	21/5	0/0	34/6
	(0.0/0.0)	(1.8/0.2)	(0.1/0.0)	(1.2/0.3)	(0.0/0.0)	(0.5/0.1)
$20 < I/\sigma \leq 30$	5/0	67/7	34/1	46/23	0/0	152/31
	(2.5/0.0)	(11.5/1.2)	(2.7/0.1)	(3.9/1.6)	(0.0/0.0)	(2.9/0.6)
$10 < I/\sigma \leq 20$	38/0	245/41	303/65	268/109	5/1	859/216
	(21.7/0.0)	(47.2/7.1)	(25.6/5.0)	(19.4/7.9)	(0.2/0.0)	(16.5/4.0)
$7 < I/\sigma \leq 10$	22/0	134/64	308/74	247/113	33/2	744/253
	(32.8/0.0)	(66.7/16.4)	(48.9/10.6)	(33.6/14.5)	(1.6/0.1)	(28.3/8.0)
$5 < I/\sigma \leq 7$	33/2	100/67	278/122	279/170	61/18	751/379
	(49.5/1.0)	(81.2/26.2)	(70.0/19.8)	(49.8/24.3)	(4.2/0.9)	(40.2/14.0)
$3 < I/\sigma \leq 5$	31/21	74/144	236/299	375/306	259/78	975/848
	(65.2/11.6)	(92.0/47.1)	(87.9/42.5)	(71.5/42.0)	(15.0/4.2)	(55.6/27.4)
$2 < I/\sigma \leq 3$	27/15	30/114	88/283	226/338	364/157	735/907
	(78.8/19.2)	(96.4/63.7)	(94.6/63.9)	(84.5/61.5)	(30.3/10.7)	(67.3/41.8)
$1 < I/\sigma \leq 2$	26/53	20/154	56/324	193/416	799/723	1094/1670
	(91.9/46.0)	(99.3/86.1)	(98.8/88.4)	(95.7/85.6)	(63.8/41.1)	(84.6/68.2)
$0 < I/\sigma \leq 1$	16/96	5/92	16/150	74/244	823/1331	934/1913
	(100.0/94.4)	(100.0/99.4)	(100.0/99.8)	(99.9/99.7)	(98.3/96.9)	(99.4/98.5)
Negative peaks	0/11	0/4	0/3	1/6	40/74	41/98
	(100.0/100.0)	(100.0/100.0)	(100.0/100.0)	(100.0/100.0)	(100.0/100.0)	(100.0/100.0)
Overall	198/198	687/688	1320/1321	1730/1730	2384/2384	6319/6321

Numbers are the number of reflections found in each range of I/σ and resolution, and numbers in parentheses are the percentage fractions of reflections with I/σ higher than the lower limit of each range. Each of the two statistics, with (before slash) or without (after slash) energy filtering, was obtained from 10 electron diffraction data, five of which were by the first exposure and the remaining five were by the second exposure. A total of 10 F41 crystals were used to collect all the data (see text for detail). Diffraction images were taken at 93 K with EF-2000 operated at 200 kV.

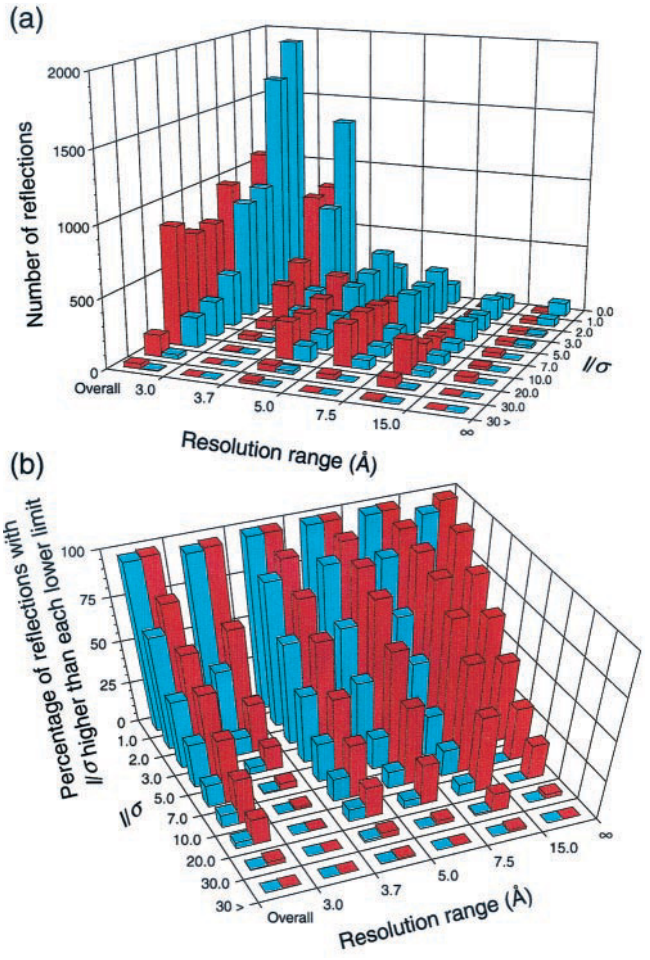

FIGURE 4 3-D representation of the intensity statistics obtained from F41 crystals with (*red bar*) and without (*blue bar*) energy filtering. (*a*) Number of reflections found within each range of I/σ and resolution. (*b*) Percentage fractions of reflections with I/σ higher than the lower limit of each range. See Table 1 for details.

There were a small number of very weak reflections for which the intensities obtained by data processing were negative because of relatively high background noises around these spots, and such reflections were eliminated from the statistics of $R_{Friedel}$ and $\Sigma R_{Friedel}$. Energy filtering actually reduced the number of such reflections.

Effect of energy filtering on 2-D crystal

The same experiments were carried out on 2-D crystals of bR. Electron diffraction patterns from a bR crystal with and without energy filtering are shown side by side in Fig. 5. With energy filtering, the level of background is significantly reduced as seen in the F41 crystal (Fig. 1). The extent of background reduction is smaller for the bR crystal than for the F41 crystal because the amount of inelastic scattering is much higher for the thicker F41 crystals, but the background reduction is still significant for bR crystals. The intensity statistics for the bR crystals are summarized in Table 3 and graphically displayed in Fig. 6, which reveals a slightly reduced but similarly significant effect of energy filtering on the quality of electron diffraction intensity data from 2-D crystals as compared with that from thin 3-D crystals. Conditions and methods for taking pairs of electron diffraction patterns from individual crystals are exactly the same as described for F41 crystals in the previous section. In low-resolution range, to 15-Å resolution, the percentage fraction of the numbers of reflections with $I/\sigma > 20$ is increased from 0% to 11.8% by energy filtering and that with $I/\sigma > 7$ is increased from 31.0% to 67.0%. If we take only reflections with $I/\sigma > 5$ and compare the percentage fractions of reflections obtained with and without energy filtering in each resolution range, as we did for the F41 crystal data, they are again all increased by energy filtering: from 42.6% to 74.1% within 15 Å; from 62.5% to 83.6% in 15 to 7.5 Å; from 10.4% to 25.3% in 7.5 to 5.0 Å; from 6.5% to 13.5% in 5.0 to 3.7 Å; from 0.0% to 0.2% in 3.7 to 3.0 Å. If we collect reflections with $I/\sigma > 2$ within a resolution range of 3.7 to 3.0 Å, the increase in the percentage fraction is from 6.7% to 11.4%. These results indicate that energy filtering is almost as effective for 2-D crystals as for thin 3-D crystals in improving the electron diffraction intensity data statistics over all resolution range out to at least 3 Å. It would probably be so beyond 3-Å resolution as suggested by the comparison of the two radial background curves shown in Fig. 5 obtained with and without energy filtering. The reduction of the background level by energy filtering amounts to ~40% at 2.8-Å resolution, which is smaller than 80% obtained for the F41 crystal data, but it is still large enough to make the accuracy of diffraction inten-

TABLE 2 $R_{Friedel}$ **factor of electron diffraction data from F41 crystals with or without energy filtering**

	Resolution range (Å)					
	∞ ~ 15	15 ~ 7.5	7.5 ~ 5.0	5.0 ~ 3.7	3.7 ~ 3.0	Overall
$R_{Friedel}$* (%)	9.4/18.0	9.3/11.4	13.3/16.1	16.2/16.9	23.5/25.6	14.3/16.3
$\Sigma R_{Friedel}$† (%)	14.2/23.5	11.7/16.6	14.3/19.1	18.4/20.4	27.3/29.7	20.1/23.2
Number of *Friedel* pairs	77/72	317/314	630/628	839/836	1126/1090	2989/2940

*$R_{Friedel} = \Sigma^n |I_{h,k} - I_{-h,-k}| / \Sigma^n (I_{h,k} + I_{-h,-k})$

†$\Sigma R_{Friedel} = \Sigma^n |(I_{h,k} - I_{-h,-k})/(I_{h,k} + I_{-h,-k})|/n$ in which summation is over n reflections with positive intensity. The statistics were obtained from the same data sets as those used for Table 1.

The values before and after slash are with and without energy filtering, respectively.

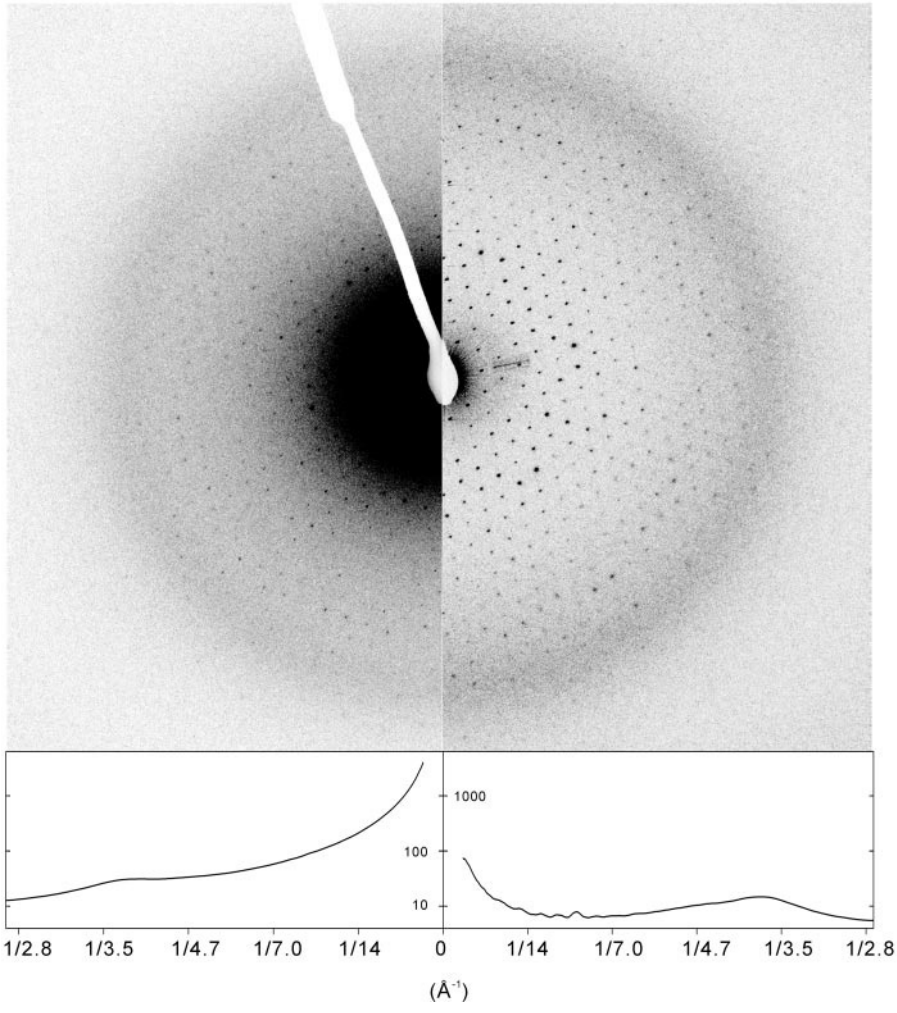

FIGURE 5 Side by side comparison of electron diffraction patterns from a 2-D crystal with and without energy filtering. The specimen is a 2-D crystal of bR ($p3$, a = 62.45 Å). The upper panels show diffraction images and the lower panels show radial background distributions (in log scale, CCD count). The left and right panels show diffraction data collected without and with energy filtering, respectively. The background intensity near the beam stop is almost 50 times higher on the left than that on the right. Even ~3-Å resolution, the background intensity without energy filtering is twice higher. The broad circular intensity at ~1/3.65 Å^{-1} from amorphous ice is more clearly seen with energy filtering.

sity data significantly higher than that without energy filtering. The level of reduction appears to extend further beyond the resolution we analyzed in the present study.

The $R_{Friedel}$ factor and $\Sigma R_{Friedel}$ factor were calculated using the same 10 data sets obtained from bR crystals (Table 4). Improvements in the standard $R_{Friedel}$ factor of the filtered data sets are not as remarkable as those seen in the F41 crystal data (Table 2), but $\Sigma R_{Friedel}$ factor values are significantly reduced out to 5.0-Å resolution.

As for the F41 crystal data, there were also a small number of very weak reflections in the bR data for which the intensities obtained by data processing were negative because of relatively high background noises around these spots, and such reflections were again eliminated from the statistics of $R_{Friedel}$ and $\Sigma R_{Friedel}$. Energy filtering reduced the number of such reflections in bR data, too.

Effect of accelerating voltage

We also examined intensity statistics obtained by using a higher accelerating voltage. Electron diffraction patterns were taken from F41 crystals and bR crystals with JEM-3000SFF, operated at 300 or 200 kV at the specimen temperature of 4 K without energy filtering. Because data collection from the same crystals was impossible by using two different microscopes and also other equipment parameters such as the electron source, detector quantum efficiency of the SSCCD, the specimen temperature, and so on are different for the two microscopes, the results obtained with JEM-3000SFF cannot be compared quantitatively with those obtained with EF-2000. It is, however, still worth comparing these data sets because the 3-D structure analysis of bR has been carried out at resolution beyond 3.0 Å by incorporating electron diffraction data collected by using JEM-3000SFF (Kimura et al., 1997; Mitsuoka et al., 1999), and therefore the quality and reliability of the diffraction data collected with this microscope under similar conditions can be treated as a standard for comparing data quality. Only data sets taken in the first exposure from five different crystals were used for the comparison.

Intensity statistics of the diffraction data from F41 crystals are summarized in Fig. 7 by plotting I/σ obtained by

TABLE 3 Data statistics of electron diffraction intensities from bR crystals with or without energy filtering

	Resolution range (Å)					
	$\infty \sim 15$	$15 \sim 7.5$	$7.5 \sim 5.0$	$5.0 \sim 3.7$	$3.7 \sim 3.0$	Overall
$I/\sigma > 30$	0/0	19/2	0/0	0/0	0/0	19/2
	(0.0/0.0)	(1.4/0.2)	(0.0/0.0)	(0.0/0.0)	(0.0/0.0)	(0.2/0.0)
$20 < I/\sigma \leq 30$	47/0	190/64	1/0	0/0	0/0	238/64
	(11.8/0.0)	(15.6/4.9)	(0.0/0.0)	(0.0/0.0)	(0.0/0.0)	(2.3/0.6)
$10 < I/\sigma \leq 20$	179/60	584/422	118/40	20/1	1/0	902/523
	(56.9/15.1)	(59.3/36.5)	(5.3/1.8)	(0.6/0.0)	(0.0/0.0)	(10.4/5.3)
$7 < I/\sigma \leq 10$	40/63	184/191	163/72	128/44	0/0	515/370
	(67.0/31.0)	(73.1/50.8)	(12.6/5.0)	(4.7/1.4)	(0.0/0.0)	(14.9/8.6)
$5 < I/\sigma \leq 7$	28/46	140/157	284/120	276/158	8/1	736/482
	(74.1/42.6)	(83.6/62.5)	(25.3/10.4)	(13.5/6.5)	(0.2/0.0)	(21.5/12.9)
$3 < I/\sigma \leq 5$	66/73	119/205	600/354	619/446	117/63	1521/1141
	(90.7/61.0)	(92.5/77.9)	(52.2/26.2)	(33.2/20.7)	(3.1/1.6)	(35.1/23.1)
$2 < I/\sigma \leq 3$	34/34	52/119	404/455	584/521	342/212	1416/1341
	(99.2/69.5)	(96.3/86.8)	(70.2/46.6)	(51.8/37.3)	(11.4/6.7)	(47.7/35.0)
$1 < I/\sigma \leq 2$	3/75	38/116	484/697	898/1158	1496/1487	2919/3533
	(100.0/88.4)	(99.2/95.4)	(91.9/77.7)	(80.4/74.1)	(48.0/43.1)	(73.8/66.6)
$0 < I/\sigma \leq 1$	0/45	11/57	178/481	592/773	2002/2189	2783/3545
	(100.0/99.8)	(100.0/99.7)	(99.8/99.2)	(99.3/98.8)	(96.9/96.5)	(98.6/98.2)
Negative peaks	0/1	0/4	4/17	23/39	126/142	153/203
	(100.0/100.0)	(100.0/100.0)	(100.0/100.0)	(100.0/100.0)	(100.0/100.0)	(100.0/100.0)
Overall	397/397	1337/1337	2236/2236	3140/3140	4092/4094	11202/11204

Numbers are the number of reflections found in each range of I/σ and resolution, and numbers in parentheses are the percentage fractions of reflections with I/σ higher than the lower limit of each range. Each of the two statistics, with (before slash) or without (after slash) energy filtering, was obtained from 10 electron diffraction data, five of which were by the first exposure and the remaining five were by the second exposure. In total, 10 bR crystals were used to collect all the data (see text for detail). Diffraction images were taken at 93 K with EF-2000 operated at 200 kV.

using EF-2000 with and without energy filtering (Fig. 7 *a*) and JEM-3000SFF operated at 200 and 300 kV (Fig. 7 *b*). At 200 kV, with energy filtering turned off in EF-2000, both microscopes produced data with similar intensity statistics. At high resolution, the data collected with JEM-3000SFF showed slightly better statistics than those collected with EF-2000, probably because the radiation damage is reduced at the specimen temperature of 4 K. But the difference was rather small.

When energy filtering is used in EF-2000, improvements in the intensity statistics are evident (Fig. 7 *a*). There are some improvements by higher voltage shown in the data sets collected with JEM-3000SFF when it is operated at 300 kV compared with those collected at 200 kV (Fig. 7 *b*), probably because of an advantage of the higher voltage for these thick specimens, but the difference is much less significant compared with energy filtering. At resolution higher than 3.4 Å, there are a few reflections in the data sets collected with JEM-3000SFF operated at 300 kV showing better I/σ than those in the filtered data sets collected with EF-2000 operated at 200 kV. However, in overall improvement, EF-2000 with energy filtering produced clearly superior diffraction data than JEM-3000 at 300 kV in every resolution range.

For 2-D crystals of bR, when the two microscopes are operated at 200 kV and energy filtering is turned off in EF-2000, the differences between the data sets collected with the two microscopes were also small (Fig. 8). The differences between the data sets collected at 200 and 300 kV were relatively small, too, probably because the advantage of the higher voltage is minimal for these thin specimens (Fig. 8 *b*). However, the data sets collected with energy filtering showed significant improvements in the intensity statistics in every resolution range (Fig. 8 *a*), although the level of improvements may be slightly smaller than that observed for the F41 crystals. All these results indicate that energy filtering has a pronounced effect for improving data statistics in electron diffraction at every resolution range regardless of the specimen thickness.

Geometric image distortions by energy filtering

Because electrons have to pass through a highly curved trajectory in the electromagnet of the energy filter for filtering, there was a strong concern that images and diffraction patterns may be distorted significantly. We therefore determined the positions of all the reflections in the diffraction patterns from F41 crystals accurately and obtained the distortion vectors that represent the geometric image distortion. In Fig. 9, such distortion vectors are plotted for both microscopes. The figures show no systematic distortion in any portion of the whole area, and the average magnitude of distortion obtained for EF-2000 with energy filtering have even smaller values than that obtained with JEM-3000SFF (Table 5). This result indicates that the amount of geometric

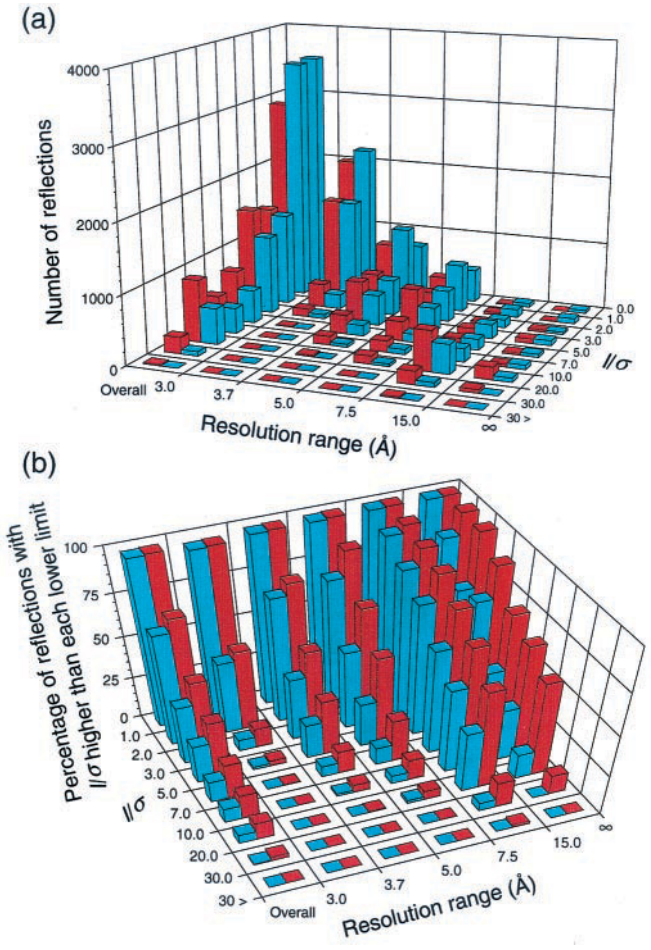

FIGURE 6 3-D representation of the intensity statistics obtained from bR crystals with (*red bar*) and without (*blue bar*) energy filtering. (*a*) Number of reflections found within each range of I/σ and resolution. (*b*) Percentage fractions of reflections with I/σ higher than the lower limit of each range. See Table 3 for details.

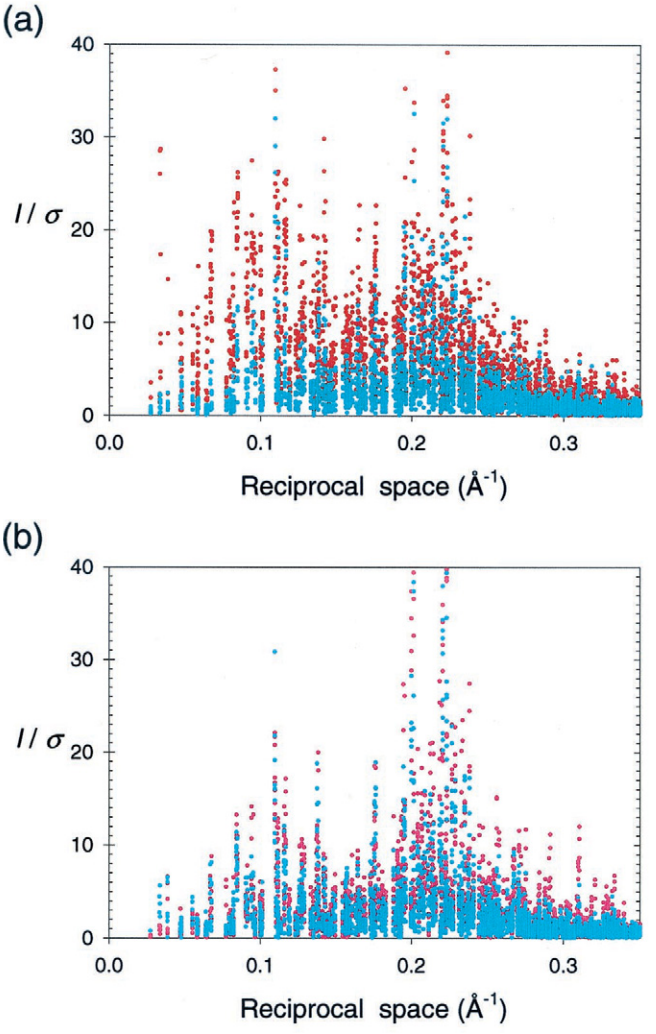

FIGURE 7 Radial distributions of I/σ comparing the quality of diffraction data from F41 crystals. (*a*) Comparison of data obtained with and without energy filtering in red and blue, respectively. Diffraction patterns were collected by using EF-2000 operated at an accelerating voltage of 200 kV and at a specimen temperature of 93 K. (*b*) Data obtained at 300 and 200 kV in magenta and blue, respectively. Diffraction patterns were collected by using JEM-3000SFF at a specimen temperature of 4 K. Each data set was obtained from five diffraction patterns from five different crystals. Only the first exposure is used.

image distortion by the γ-type energy filter in EF-2000 is negligibly small.

DISCUSSION

Effects of energy filtering

We compared electron diffraction patterns taken with and without energy filtering to quantitatively study its effect on the data quality. We collected diffraction data from thin 3-D crystals of F41 (600–750 Å thick) and 2-D monolayer

TABLE 4 $R_{Friedel}$ **factor of electron diffraction data from bR crystals with or without energy filtering**

	Resolution range (Å)					
	∞ ~ 15	15 ~ 7.5	7.5 ~ 5.0	5.0 ~ 3.7	3.7 ~ 3.0	Overall
$R_{Friedel}$* (%)	6.8/8.2	6.9/7.0	13.1/15.3	16.3/17.0	26.8/26.6	10.5/11.1
$\Sigma R_{Friedel}$† (%)	9.2/14.6	9.5/11.0	17.6/21.2	21.8/21.9	30.3/30.7	22.1/23.4
Number of *Friedel* pairs	166/165	617/613	1062/1049	1498/1482	1877/1857	5220/5166

See Table 2 for $R_{Friedel}$ and $\Sigma R_{Friedel}$. The statistics were obtained from the same data sets as those used for Table 3.
The values before and after slash are with and without energy filtering, respectively.

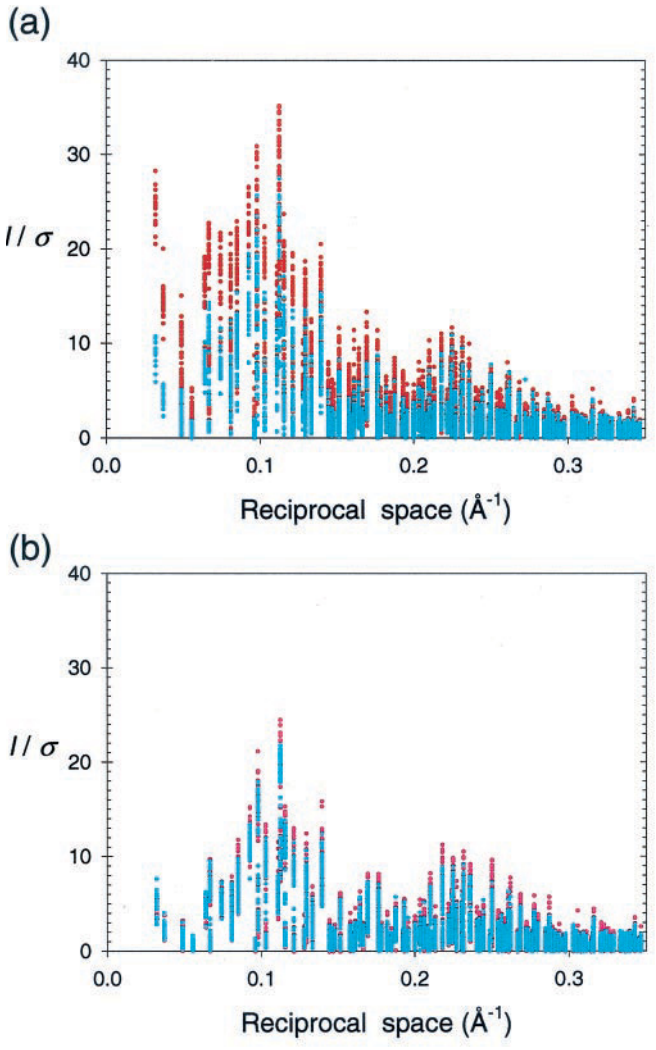

FIGURE 8 Radial distributions of I/σ comparing the quality of diffraction data from bR crystals. (*a*) Comparison of data obtained with and without energy filtering in red and blue, respectively. Diffraction patterns were collected by using EF-2000 operated at an accelerating voltage of 200 kV and at a specimen temperature of 93 K. (*b*) Data obtained at 300 and 200 kV in magenta and blue, respectively. Diffraction patterns were collected by using JEM-3000SFF at a specimen temperature of 4 K. Each data set was obtained from five diffraction patterns from five different crystals. Only the first exposure is used.

crystals of bR (~60 Å thick) to study the effect of specimen thickness. We also collected diffraction data at an accelerating voltage of 200 and 300 kV to see the difference in the data quality made by these different accelerating voltages.

For both crystals, improvements of the intensity statistics by energy filtering were remarkable in every range of resolution out to the resolution limit of the present measurement, which is 2.8 Å. It was clearly so for both F41 and bR crystals except that it was slightly less so for high-resolution data of bR crystals. The $R_{Friedel}$ factor and $\Sigma R_{Friedel}$ factor also showed similar results (Tables 2 and 5). Because F41 crystals are ~10 times thicker than bR crystals, these results indicate a certain advantage of energy filtering for thicker specimens, and this is consistent with the fact that thicker specimens produce more inelastic electrons.

It was generally believed that inelastic scattering contributes only to low-resolution data. The intensity of inelastic scattering is in fact orders of magnitude higher than that of elastic scattering at low resolution, but it falls off rapidly as the resolution become higher. Therefore, the remarkable improvement of the intensity statistics at low resolution by removal of the high background intensity by energy filtering is just as expected. Angert et al. (1996), however, have shown that there is significantly high background in electron diffraction patterns from vitreous ice in high scattering angle region. Accordingly, we observed high levels of background intensities and noises in all resolution ranges out to ~3 Å (Figs. 1, 2, and 5) and quantitatively showed that energy filtering is effective in removing most of these high background intensities and noises (Tables 1 and 3; Figs. 4 and 6). Thus, the advantage of energy filtering at high resolution is much greater than previously supposed. This is probably because the background intensity has a significant contribution from elastic-inelastic double scattering, particularly at high resolution, and energy filtering is effective in removing the double scattering as well as the single inelastic scattering.

Although it is possible to subtract a smooth background intensity distribution under the reflections in unfiltered data sets, the background noises by inelastic scattering cannot be removed by any sophisticated background correction procedure in the same way as energy filtering, because a relatively high level of statistical noises is intrinsic to the background (Fig. 2) and these noises are always superimposed on the peak profile of each reflection. Moreover, elastic-inelastic double scattering would also be counted in the integrated intensity of Bragg reflections in unfiltered data. Somewhat broader peak profiles observed in unfiltered data sets than those in filtered data sets may indicate the presence of such double scattering. Therefore, subtraction of a locally smoothed background surface (Mitsuoka et al., 1999) cannot reduce these noises nor remove such energy-loss double scattered electrons from integrated spot intensity as energy filtering does. This results in lower I/σ (Figs. 3, 4, and 6; Tables 1 and 3) and larger $R_{Friedel}$ factor and $\Sigma R_{Friedel}$ factor (Tables 2 and 4) in unfiltered electron diffraction data. Improvements in the intensity data statistics, for instance, I/σ, by removal of inelastic scattering by energy filtering are more or less consistent with those predicted from the removed background intensity, although the values obtained are somewhat less than those predicted.

Comparison of the $R_{Friedel}$ factor and $\Sigma R_{Friedel}$ factor showed that energy filtering is more effective in improving the data quality of weak reflections, which is useful because strong reflections already have good data statistics. In this report, we examined only partially hydrated crystals, but

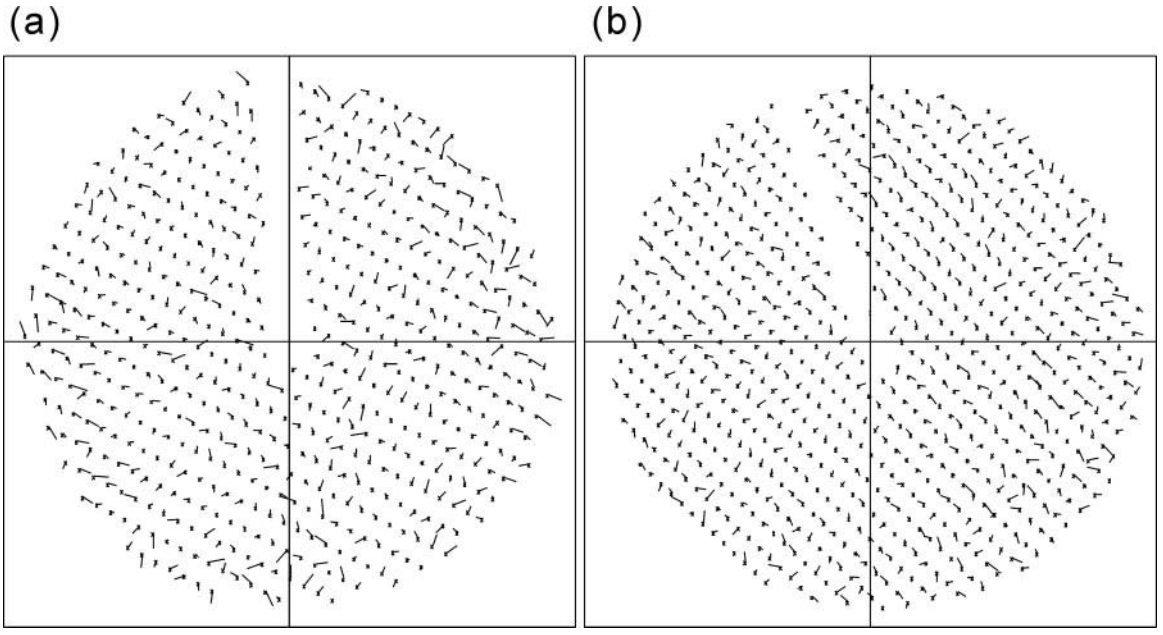

FIGURE 9 Effect on the geometric image distortion by γ-shaped electron trajectory within the EF-2000 energy filter unit. (*a*) Lattice image distortion observed by JEM-3000SFF. (*b*) Lattice image distortion observed by EF-2000, in which the trajectory of electrons are γ-shaped within its energy filter unit. Deviations of the positions of reflections from the ideal ones were obtained from diffraction patterns from F41 crystals, and deviation vectors are drawn on corresponding reflections to represent the lattice image distortion. Deviation vectors are magnified by a factor of 20. Note that the magnitudes of geometric distortion are comparable for both microscopes, indicating that there is no significant geometric image distortion produced by the energy filter unit of EF-2000 (see also Table 5).

improvements would be larger for fully hydrated samples embedded in thicker ice.

Accelerating voltage and specimen temperature

We compared the advantage of energy filtering to a higher accelerating voltage in the amount of improvement in the quality of diffraction data. The results showed that the improvement by energy filtering is much more prominent than that observed by use of an accelerating voltage of 300 kV instead of 200 kV (Figs. 7 and 8). The only exception was in a high-resolution region beyond 3.4 Å, where some reflections in the unfiltered data sets from F41 crystals collected at 300 kV showed a slightly better I/σ than those in the filtered data sets collected at 200 kV (Fig. 7). The scattering cross-section of light atoms by 300 keV electron is ~0.8 times of the one by 200-keV electron, which means that 300 keV electrons have 1.25 times more power of penetration through the specimen. Therefore, the use of 300 kV reduces the probability of dynamical scattering in thick specimens and presumably results in more reflections with better I/σ at high resolution as compared with the use of 200 kV. Even with this advantage of higher accelerating voltage, overall performance of energy filtering proved to surpass the higher voltage in improving the data quality significantly.

In the present study, we did not carefully examine the effect of radiation damage on the data quality. The radiation damage is presumably more reduced at liquid helium temperature in the specimen stage of JEM-3000SFF compared

TABLE 5 Statistics of lattice distortions in diffraction data from F41 crystals collected with JEM-3000SFF or EF-2000, shown in Fig. 9

	Δx (p.u.)	Δy (p.u.)	Δr (p.u.)
1st Quadrant	0.065/−0.075	0.213/0.172	1.027/1.036
2nd Quadrant	0.208/−0.129	0.334/−0.256	1.283/1.179
3rd Quadrant	−0.021/0.095	−0.090/0.322	1.167/1.243
4th Quadrant	−0.026/0.105	0.165/−0.183	1.182/0.934
Whole	0.055/0.002	0.151/0.016	1.167/1.103

Data shown as Δx and Δy are the x and y component of deviation vectors, respectively, and Δr is the magnitude of deviation vectors, all averaged over each quadrant of the electron diffraction images or over the whole images, and presented in pixel unit of the CCD (p.u.).
Data before and after slash are those obtained by JEM-3000SFF and EF-2000, respectively.

with that at liquid nitrogen temperature in the specimen holder used in EF-2000 (Fujiyoshi et al., 1986). Therefore, the data collected by JEM-3000SFF should have another factor of advantage in having better quality, but it was not manifest in the data statistics. The difference by temperature did not show up clearly probably because we collected electron diffraction data with a very small amount of dose ($1 \sim 2$ $e^-/Å^2$) and the effect of radiation damage would have been minimal.

Image distortion by the γ-type energy filter

Potential image distortion was a concern with energy filtering because scattered electrons travel through highly bent trajectories in the energy filter electromagnet. However, the magnitude of distortion produced by the γ-type filter in EF-2000 was negligibly small, and no systematic distortion was observed, as revealed in the comparison with the distortion data obtained in the same way with JEM-3000SFF, which does not have an energy filter (Fig. 9). The statistics of geometric distortions actually showed that the magnitude of image distortion is slightly smaller in EF-2000 even with the energy filter than that obtained by JEM-3000SFF (Table 5). This means that image data collected with energy filtering can be processed and used without any distortion correction for high-resolution structure analysis. Collection of diffraction intensity data can be carried out accurately because diffraction spots can be located with minimal positional errors in data processing procedures. The γ-type energy filter system in EF-2000 would thus be a powerful tool that enables accurate data collection for both electron diffraction and imaging from low to high resolution.

Perspectives

Electron crystallography, which uses structure amplitude data from electron diffraction and phase data obtained by image processing, is capable of visualizing atomic details of the 3-D structures of protein molecules when well-ordered 2-D crystals are available (Henderson et al., 1990; Kühlbrandt et al., 1994; Kimura et al., 1997; Nogales et al., 1998; Murata et al., 2000). Once the atomic models are built, refinement of the models and further extension of resolution can be carried out using electron diffraction data alone (Mitsuoka et al., 1999). Accurate amplitude data collection by electron diffraction from 2-D crystals of proteins, either in different conformational states or with ligand molecules bound, allows the visualization of conformational changes or bound ligand molecules in their binding sites (Subramaniam and Henderson, 2000; Vonck, 2000; Downing and Li, 2001). Thus, electron diffraction is potentially a very powerful tool in molecular and cellular biology.

In principle, the power of electron crystallography is not limited only to monolayer 2-D crystals. Application of the method can be extended to thin 3-D crystals for which even recent technological advancements in x-ray crystallography do not have enough power to do anything. So many protein structures have actually been and are being solved at high resolution by x-ray crystallography by virtue of dedicated synchrotron radiation beam lines that provide brilliant x-ray beams with variable wavelength, cryocrystallographic methods that allow collection of multiple data set from just one single protein crystal, and availability of good 2-D detector such as the image plate and CCD. Relatively easy construction of overexpression systems for target proteins by genetic techniques also helps provide pure protein samples in large enough amounts for rapid crystallization screening. However, quite often we still encounter a situation where crystallization trials give rise to only thin and tiny 3-D crystals that are still difficult to collect x-ray diffraction data from even with a strong x-ray beam from synchrotron. In principle, electron crystallography has a high potential to solve the structure of such thin crystals.

There have been several trials to solve the structure of such thin crystals by electron crystallography, but none has succeeded to date due to technical difficulties (Shi et al., 1998). Multiple elastic scattering (dynamical scattering) of electrons has been thought as the most fatal problem (Ho et al., 1988). However, the mean free path of elastically scattered electrons in ice was measured to be ~2800 Å at 120 kV (Angert et al., 1996). At an accelerating voltage of 200 kV, the mean free path will be 1.4 times longer than that at 120 kV. Therefore, even though the mean free path of electrons in proteins would be a little shorter than that in ice, multiple elastic scattering might not be so serious for 3-D crystals with thickness less than 2000 Å.

The mean free path of inelastically scattered electrons in ice was measured to be ~800 Å (Angert et al., 1996), which is much shorter than that of elastic electrons. That is why the level of background intensity by inelastic electrons is relatively high compared with diffraction spot intensities by elastic electrons. This high and noisy background extends even to high resolution (Figs. 1, 2, and 5), causing a serious problem in collecting accurate diffraction intensity data. As electron crystallography requires diffraction data to be collected also from highly tilted crystals (up to 70°), for which the effective thickness of the crystals increases up to twice or more of the actual thickness, this would increase the background intensity and noise further. But, energy filtering can effectively remove most of these inelastic electrons as demonstrated in the present study.

Another problem in electron crystallography is that the crystallographic R factors in the refinement of atomic models tend to be significantly worse than those obtained by x-ray crystallography. Some efforts have been made to improve the situation by incorporating the distribution of charges in modification of atomic scattering factors used

in x-ray crystallography (Mitsuoka et al., 1999), and it actually helps improve the *R* factor because electrons are diffracted by the potential distribution and not the electron density distribution by which x-ray photons are diffracted. A more careful data processing procedure, incorporating a peak profile fitting technique as partially implemented in our present study, will also help improve the data accuracy significantly. But, even with these technical improvements in the refinement and data processing procedure, the *R* factors are still relatively poor, and it is most likely caused by relatively poor signal to noise ratio of electron diffraction images. For weak reflections, particularly at high resolution, the poor signal to noise ratio comes mainly from relatively low electron counts for reflection peaks, as indicated by relatively high $R_{Friedel}$ factor and $\Sigma\ R_{Friedel}$ factor and their small improvements by energy filtering at high resolution, particularly with two-dimensional crystal, as shown in Table 2 and 4. In the present experiments, however, all the diffraction data were collected with a total electron dose limited to $\sim$1 $e^-/Å^2$ and from an area limited to a diameter of $\sim$1.2 μm, and at least the dose can be further increased to obtain much better intensity statistics. Even then, accurate measurement of intensities would be hampered by the high background noises produced by inelastically scattered electrons. Therefore, by removing such inelastic electrons, *R* factors should substantially be improved. In addition, accurate measurement of low-resolution data ($<1/5$ $Å^{-1}$) will lead to a better visualization of the charge distribution, where the effects of polarization in molecules are relatively large (Mitsuoka et al. 1999). Significant improvements by energy filtering in the $R_{Friedel}$ factor and $\Sigma\ R_{Friedel}$ factor as well as in the statistics of I/σ over all resolution ranges out to 3 Å, as demonstrated in the present study, particularly for thicker crystals and weak reflections, clearly indicate that energy filtering will give great advantages for more accurate structure analysis of proteins embedded in ice by electron crystallography.

There would also be a significant benefit in the image mode by energy filtering. In the image mode, the inelastically scattered electrons contribute to the shot noise in the image background, because they have a white spectrum in the Fourier transform. Our preliminary measurements showed that the background reduction in image data by energy filtering amounts to 30% to 50% or more depending on the thickness of the specimen. This will reduce the shot noise as well and increase the signal to noise ratio of image data significantly. Therefore, energy filtering would also be beneficial for more accurate image data collection, which will certainly facilitate high-resolution structure analysis of macromolecular complexes embedded in ice by single particle image analysis and helical image reconstruction.

We thank F. A. Samatey, N. Gyobu and Y. Fujiyoshi for kindly giving us F41 and bR samples, respectively, T. Hirai for his instruction on the use of their programs for electron diffraction data processing, C. Toyoshima and Y. Taniguchi for helpful advice on the use of the energy filtering electron microscope, and T. Nitta and F. Oosawa for continuous support and encouragement.

REFERENCES

Angert, I., C. Burmester, C. Dinges, H. Rose, and R. R. Schröder. 1996. Elastic and inelastic scattering cross-sections of amorphous layers of carbon and vitrified ice. *Ultramicroscopy.* 63:181–192.

Angert, I., E. Majorovits, and R. R. Schröder. 2000. Zero-loss image formation and modified contrast transfer theory in EFTEM. *Ultramicroscopy.* 81:203–222.

Auer, M., G. A. Scarborough, and W. Kühlbrandt. 1999. Surface crystallisation of the plasma membrane H^+-ATPase on a carbon support film for electron crystallography. *J. Mol. Biol.* 287:961–968.

Baldwin, J., and R. Henderson. 1984. Measurement and evaluation of electron diffraction patterns from two-dimensional crystals. *Ultramicroscopy.* 14:319–336.

Downing, K. H., and H. Li. 2001. Accurate recording and measurement of electron diffraction data in structural and difference Fourier studies of proteins. *Microsc. Microanal.* 7:407–417.

Fujiyoshi, Y., N. Uyeda, H. Yamagishi, K. Morikawa, T. Mizusaki, Y. Aoki, H. Kihara, and Y. Harada. 1986. Biological macromolecules observed with high resolution cryo-electron microscope. *Proc. 11th Int. Congr. Electron Microsc. Kyoto.* 3:1829–1832.

Henderson, R., J. M. Baldwin, T. A. Ceska, F. Zemlin, E. Beckmann, and K. H. Downing. 1990. An atomic model for the structure of bacteriorhodopsin. *J. Mol. Biol.* 213:899–929.

Hirai, T., K. Murata, K. Mitsuoka, Y. Kimura, and Y. Fujiyoshi. 1999. Trehalose embedding technique for high-resolution electron crystallography: application to structural study on bacteriorhodopsin. *J. Electron Microsc.* 48:653–658.

Ho, M. H., B. K. Jap, and R. M. Glaeser. 1988. Validity domain of the weak-phase-object approximation for electron diffraction of thin protein crystals. *Acta Crystallogr.* A44:878–884.

Kimura, Y., D. G. Vassylyev, A. Miyazawa, A. Kidera, M. Matsushima, K. Mitsuoka, K. Murata, T. Hirai, and Y. Fujiyoshi. 1997. Surface of bacteriorhodopsin revealed by high-resolution electron crystallography. *Nature.* 389:206–211.

Kühlbrandt, W., D. N. Wang, and Y. Fujiyoshi. 1994. Atomic model of plant light-harvesting complex by electron crystallography. *Nature.* 367: 614–621.

Langmore, J. P., and M. F. Smith. 1992. Quantitative energy-filtered electron microscopy of biological molecules in ice. *Ultramicroscopy.* 46:349–373.

Misell, D. L., and E. B. Brown. 1987. Electron Diffraction: An Introduction for Biologist. Elsevier, Amsterdam.

Mitsuoka, K., T. Hirai, K. Murata, A. Miyazawa, A. Kidera, Y. Kimura, and Y. Fujiyoshi. 1999. The structure of bacteriorhodopsin at 3.0 Å resolution based on electron crystallography: implication of the charge distribution. *J. Mol. Biol.* 286:861–882.

Murata, K., K. Mitsuoka, T. Hirai, T. Walz, P. Agre, J. B. Heymann, A. Engel, and Y. Fujiyoshi. 2000. Structural determinants of water permeation through aquaporin-1. *Nature.* 407:599–605.

Nogales, E., S. G. Wolf, and K. H. Downing. 1998. Structure of the $\alpha\beta$ tubulin dimer by electron crystallography. *Nature.* 391:199–203.

Samatey, F. A., K. Imada, S. Nagashima, F. Vonderviszt, T. Kumasaka, M. Yamamoto, and K. Namba. 2001. Structure of the bacterial flagellar protofilament and implications for a switch for supercoiling. *Nature.* 410:331–337.

Samatey, F. A., K. Imada, F. Vonderviszt, Y. Shirakihara, and K. Namba. 2000. Crystallization of the F41 fragment of flagellin and data collection from extremely thin crystals. *J. Struct. Biol.* 132:106–111.

Shi, D., M. R. Lewis, H. S. Young, and D. L. Stokes. 1998. Three-dimensional crystals of Ca^{2+}-ATPase from sarcoplasmic reticulum: merging electron diffraction tilt series and imaging the (*h*. *k* 0) projection. *J. Mol. Biol.* 284:1547–1564.

Subramaniam, S., and R. Henderson. 2000. Molecular mechanism of vectorial proton translocation by bacteriorhodopsin. *Nature.* 406: 653–657.

Taya, S., Y. Taniguchi, E. Nakazawa, and J. Usukura. 1996. Development of γ-type energy filtering TEM. *J. Electron Microsc.* 45:307–313.

Toyoshima, C., H. Ogawa, and K. Tani. 1998. Energy-filtering electron crystallography of proteins. Hitachi Instrument News, the33rd Electron Microscopy Edition. Hitachi, Ltd., Tokyo. 3–7.

Vénien-Bryan, C., G. F. Schertler, E. Thouvenin, and S. Courty. 2000. Projection structure of a transcriptional regulator, HupR, determined by electron cryo-microscopy. *J. Mol. Biol.* 296:863–871.

Vonck, J. 2000. Structure of the bacteriorhodopsin mutant F219L N intermediate revealed by electron crystallography. *EMBO J.* 19: 2152–2160.

Zhu, J., P. A. Penczek, R. Schröder, and J. Frank. 1997. Three-dimensional reconstruction with contrast transfer function correction from energy-filtered cryoelectron micrographs: procedure and application to the 70S *Escherichia coli* ribosome. *J. Struct. Biol.* 118:197–219.